THE JOURNAL OF BIOLOGICAL CHEMISTRY
Vol. 279, No. 21, Issue of May 21, pp. 22258–22266, 2004
Printed in U.S.A.

A Fluorescence Cell Biology Approach to Map the Second Integrin-binding Site of Talin to a 130-Amino Acid Sequence within the Rod Domain*

Received for publication, January 28, 2004, and in revised form, March 17, 2004
Published, JBC Papers in Press, March 18, 2004, DOI 10.1074/jbc.M400947200

Laurent Tremuth‡§, Stephanie Kreis‡, Chantal Melchior‡, Johan Hoebeke¶, Philippe Rondé‖, Sébastien Plançon‡, Kenneth Takeda‖, and Nelly Kieffer‡ ‡‡**

*From the ‡Laboratoire de Biologie et Physiologie Intégrée (CNRS/GDRE-ITI), Université du Luxembourg, 162A, Avenue de la Faïencerie, L-1511, Luxembourg, ¶Immunologie et Chimie Thérapeutiques (UPR 9021 CNRS), Institut de Biologie Moléculaire et Cellulaire, Strasbourg 67000, France, ‖Pharmacologie et Physicochimie des Interactions Cellulaires et Moléculaires (UMR CNRS 7034), Université Louis Pasteur de Strasbourg, Illkirch 67401, France, and **Institut Gilbert Laustriat (IFR 85), Illkirch 67401, France*

The cytoskeletal protein talin, which provides a direct link between integrins and actin filaments, has been shown to contain two distinct binding sites for integrin β subunits. Here, we report the precise delimitation and a first functional analysis of the talin rod domain integrin-binding site. Partially overlapping cDNAs covering the entire human talin gene were transiently expressed as DsRed fusion proteins in Chinese hamster ovary cells expressing $\alpha_{IIb}\beta_3$, linked to green fluorescent protein (GFP). Two-color fluorescence analysis of the transfected cells, spread on fibrinogen, revealed distinct subcellular staining patterns including focal adhesion, actin filament, and granular labeling for different talin fragments. The rod domain fragment G (residues 1984–2344), devoid of any known actin- or vinculin-binding sites, colocalized with β_3-GFP in focal adhesions. Direct *in vitro* interaction of fragment G with native platelet integrin $\alpha_{IIb}\beta_3$ or with the recombinant wild type, but not the Y747A mutant β_3 cytoplasmic tail, linked to glutathione *S*-transferase, was demonstrated by surface plasmon resonance analysis and pull-down assays, respectively. Here, we demonstrate for the first time the *in vivo* relevance of this interaction by fluorescence resonance energy transfer between β_3-GFP and DsRed-talin fragment G. Further *in vitro* pull-down studies allowed us to map out the integrin-binding site within fragment G to a stretch of 130 residues (fragment J, residues 1984–2113) that also localized to focal adhesions. Finally, we show by a cell biology approach that this integrin-binding site within the talin rod domain is important for β_3-cytoskeletal interactions but does not participate in $\alpha_{IIb}\beta_3$ activation.

Integrin-mediated cell adhesion and signaling are crucial events for numerous biological processes such as morphogenesis, the immune response, hemostasis, cell growth, and differentiation as well as for cell survival (1). Integrins function as noncovalent $\alpha\beta$ heterodimeric transmembrane receptors that link the extracellular matrix to the actin cytoskeleton; they are, however, unable to directly interact with actin filaments. A number of actin-binding proteins, including talin, α-actinin, filamin, myosin, and skelemin, have been identified that act as intermediates in connecting integrins to the actin cytoskeleton (2). Among these, talin was the first intracellular ligand shown to interact directly with integrin β-subunit cytoplasmic tails (3).

Talin is a multifunctional ~270-kDa (2541 amino acids) cytoskeletal protein that forms antiparallel homodimers, which represent the biologically active form of the protein (4). *In vivo*, talin is found in equilibrium between a membrane-bound and a cytoplasmic form (4, 5), and several studies have emphasized its role in regulating integrin-actin cytoskeleton complexes (6) and integrin activation (7, 8). Talin colocalizes with integrins at sites of cell-matrix interactions and membrane ruffles of moving cells (9, 10), and it is necessary for the assembly of focal adhesions (FAs).[1] The functional role of talin has been elucidated by antibody inhibition studies and genetic approaches. Microinjection of anti-talin antibodies into fibroblasts led to the disruption of FAs and associated stress fibers (11), and down-regulation of talin by antisense mRNA or short hairpin RNAs reduced cell spreading and FA assembly in HeLa cells, integrin processing and transport to the cell surface, and energy-dependent integrin activation (8, 12, 13). Disruption of the *Talin1* gene by a knockout approach in mice revealed that undifferentiated *Talin1* (−/−) embryonic stem cells exhibited defective cell adhesion and spreading and were unable to assemble FAs or stress fibers, whereas differentiated cells readily formed these adhesion complexes (14). The only partially inhibitory phenotype observed in *Talin1* (−/−) mouse fibroblast-like cells may be explained by the presence of a second, recently identified *TALIN2* gene in mammalian cells (15). Indeed, in *Drosophila*, disruption of the *rhea* locus, which corresponds to the unique talin gene, mimics the integrin knockout phenotype, underlining the important role of talin as an obligatory component of integrin-mediated adhesion (16).

* This work, which was carried out as a joint project in the context of the CNRS European network "Integrins and Transfer of Information" (GDRE-ITI), was supported by the University of Luxembourg, Fonds National de la Recherche Grant FNR 01/04/06, the Fondation Luxembourgeoise Contre le Cancer, and EC Grant HPRN-CT-2002-00253. Data presented here were obtained as part of the doctoral thesis of L. T. to be submitted to the University Louis Pasteur, Strasbourg. The costs of publication of this article were defrayed in part by the payment of page charges. This article must therefore be hereby marked "*advertisement*" in accordance with 18 U.S.C. Section 1734 solely to indicate this fact.

§ Supported by a fellowship from the Ministère de la Culture, de l'Enseignement Supérieur et de la Recherche, Luxembourg.

‡‡ To whom correspondence should be addressed. Tel.: 352-466644440; Fax: 352-466644442; E-mail: kieffer@cu.lu.

[1] The abbreviations used are: FA, focal adhesion; FRET, fluorescence resonance energy transfer; SPR, surface plasmon resonance; CHO, Chinese hamster ovary; GST, glutathione *S*-transferase; GFP, green fluorescent protein; PBS, phosphate-buffered saline; IMDM, Iscove's modified Dulbecco's medium; Pipes, 1,4-piperazinediethanesulfonic acid; TRITC, tetramethylrhodamine isothiocyanate; bis-Tris, 2-[bis-(2-hydroxyethyl)amino]-2-(hydroxymethyl)propane-1,3-diol.

In living cells, talin can be cleaved into a globular 47-kDa N-terminal head domain and an elongated 190-kDa C-terminal rod domain by the calcium-dependent protease calpain II (17). The talin head (residues 1–433), which includes a region (residues 86–410) homologous to the N-terminal FERM domain of the band 4.1, ezrin, radixin, moesin family of cytoskeletal proteins (17), contains an actin-binding site (18), three potential membrane-association sites (19, 20), and binding sites for integrins, layilin, focal adhesion kinase, myosin (21), and type 1γ phosphatidylinositol phosphate kinase (22). The binding affinity of talin for integrins increases upon calpain cleavage or in the presence of phosphatidylinositol 4,5-biphosphate, suggesting that conformational changes within talin unmask cryptic integrin-binding sites (13, 23). Recent biochemical (7, 24), crystallographic, and NMR studies (25, 26) have mapped the integrin-binding site in the talin head fragment to a mainly hydrophobic area in the F3 subdomain of the FERM domain. Recombinant F3, which binds integrin tails with a similar affinity as the talin head domain (7), functions as a phosphotyrosine-binding domain (25), recognizing the ^{744}NP*X*Y^{747} motif in the β_3 cytoplasmic tail. Residue Tyr^{747} appears to be critical for this interaction, since the Y747A mutation abrogates the talin head binding to the β subunit (24). Binding of the talin head domain to the cytoplasmic tail of integrin β subunits leads to integrin activation (8), and this was shown by overexpression of the F3 subdomain of the talin FERM domain in CHO $\alpha_{IIb}\beta_3$ cells, which results in increased binding of the ligand mimetic anti-$\alpha_{IIb}\beta_3$ antibody PAC-1 (7, 24).

The talin rod domain is composed of multiple α-helical alanine-rich repeats (27) and contains a dimerization site (28), an integrin-binding site (3, 29), three vinculin-binding sites (30), a recently identified TES-binding site (31), and two actin-binding sites, the C-terminal one of which is highly conserved among actin-binding proteins (32, 33). Using *in vitro* solid phase binding assays, the β_3 integrin-binding site of the rod domain has recently been shown to be contained within a recombinant fragment encoding the 558 C-terminal residues of talin (29).

The functional significance of the interaction between the talin rod domain and the β-subunit of integrins in integrin-mediated cell adhesion and spreading remains largely unknown. In order to study this specific interaction, we have used a cell biology and a biochemical approach to map the integrin-binding site in the talin rod domain to a polypeptide of 130 amino acids, located between the C-terminal actin- and vinculin-binding sites. We also provide evidence that in FAs this fragment directly interacts with the cytoplasmic tail of β_3 but that this interaction does not participate in integrin activation.

EXPERIMENTAL PROCEDURES

Protein Expression and Affinity Purification—Talin cDNA fragments encoding amino acids 1–433 (fragment A), 430–1076 (fragment B), 1984–2541 (fragment F), and 1984–2344 (fragment G) were amplified by reverse transcriptase-PCR using human erythroleukemic HEL cell mRNA; cDNA fragments encoding amino acids 1984–2270 (fragment H), 1984–2113 (fragment J), and 2093–2344 (fragment K) were amplified by PCR from the talin G construct. The primers used for PCR amplification were designed to generate appropriate restriction sites allowing the cloning of the amplified cDNAs into the pGEX-4T-2 vector (Amersham Biosciences); for fragment A, SalI and EcoRI restriction sites were generated at the 5′- and 3′-ends, respectively; all remaining fragments were cloned using a single SalI site, and their orientation in the vector was determined by PCR. Fidelity of all cloned talin cDNA fragments with the human talin sequence (GenBank™ AF078828) was confirmed by automated sequencing (Applied Biosystems). Expression of GST fusion proteins in *Escherichia coli* BL21(DE3) was induced with 0.2 mM isopropyl-1-thio-β-D-galactopyranoside for 3 h at 37 °C. Cells were lysed as previously described (34). Fusion proteins from the soluble fraction were affinity-purified on glutathione-Sepharose 4B beads according to the manufacturer's instructions (Amersham Biosciences) and finally dialyzed against PBS. Talin fragments used for surface plasmon resonance analysis were cleaved from the GST tag by thrombin digestion (10 units/mg of protein, Amersham Biosciences) for 1 h at room temperature. Thrombin was neutralized with phenylmethylsulfonyl fluoride (1 mM), and the fragments were dialyzed against PBS.

cDNA fragments encoding the cytoplasmic tail of wild type β_3 or the β_3Y747A mutant (residues 716–762) were generated from the corresponding full-length constructs (35) using primers introducing BamHI and SmaI restriction sites at the 5′- and 3′-ends, respectively. These fragments were ligated into the pGEX-4T-2 vector, and the corresponding GST-fusion proteins were expressed and purified as described above.

For expression of talin fragments in CHO $\alpha_{IIb}\beta_3$-GFP cells, recombinant DsRed fusion proteins of human talin were generated by cloning the cDNA of talin fragment A into the SalI and SacI and the cDNAs of all the other talin fragments into the SalI and BamHI restriction sites of the pDsRed-N1 vector (Clontech), resulting in fragments covering talin residues 1–433 (fragment A), 430–1076 (fragment B), 1075–1623 (fragment C), 1622–2270 (fragment D), 2267–2541 (fragment E), 1984–2541 (fragment F), 1984–2344 (fragment G), 1984–2270 (fragment H), 2267–2344 (fragment I), 1984–2113 (fragment J), 2093–2344 (fragment K), and 2093–2270 (fragment L). For integrin activation studies by flow cytometry, GFP fusion proteins of talin fragments A, G, and J were generated by cloning the corresponding cDNAs into the pEGFP-N1 vector using SalI and BamHI restriction sites. Furthermore, the cDNA encoding talin residues 1977–2113 was also inserted into the pcDNA4/TO/*myc*-His vector (Invitrogen) using BamHI and EcoRI restriction sites, generating a recombinant protein with a C-terminal *myc*-His tag (J_{myc}).

Cell Transfection and Indirect Immunofluorescence—CHO cells, stably transfected with $\alpha_{IIb}\beta_3$-GFP (36), or HT-144 human melanoma cells (ATCC HTB 63) were cultured in IMDM supplemented with 10% fetal calf serum, 2 mM glutamine, 100 units/ml penicillin, and 100 μg/ml streptomycin and were transfected as previously described (35). Briefly, for each cDNA construct, 1.5×10^6 adherent cells were transfected with 3–15 μg of cDNA using LipofectAMINE™ (Invitrogen) according to the manufacturer's instructions. Fetal calf serum (10% final concentration) was added after 24 h, and 48 h after transfection, cells were detached with EDTA buffer (50 mM Hepes, 126 mM NaCl, 5 mM KCl, 1 mM EDTA, pH 7.5), washed, resuspended in serum-free IMDM, and seeded onto glass coverslips coated with fibrinogen (20 μg/ml). After 2 h of adhesion at 37 °C, cells were fixed for 15 min at 4 °C in fixation buffer (PBS, pH 7.4, 3% paraformaldehyde, 2% sucrose) and washed four times in washing buffer (PBS, pH 7.4, 0.5% Triton X-100, 0.5% bovine serum albumin).

For indirect immunofluorescence staining of the *myc*-tagged fragment J, the fixed cells were incubated for 40 min with a monoclonal mouse anti-*myc* antibody (9B11, 0.5 μg/ml; Cell Signaling) and for 30 min with a rhodamine (TRITC)-conjugated goat anti-mouse IgG antibody (7.5 μg/ml; Jackson ImmunoResearch Laboratories, Inc.). After each incubation step, the coverslips were washed three times for 5 min in washing buffer. Finally, the coverslips were mounted on microscopy slides in Mowiol/DABCO (Sigma).

Fluorescence Microscopy and Fluorescence Resonance Energy Transfer (FRET) Analysis—For fluorescence analysis, GFP- and DsRed-conjugated proteins were visualized in paraformaldehyde-fixed cells adherent on fibrinogen-coated glass coverslips. Single images were collected under a conventional fluorescence microscope (LEICA Leitz DMRB) with a 63× oil immersion objective and a LEICA DC 300F camera using the LEICA IM1000 1.20 software. Images were processed digitally with Photoshop 6.0 (Adobe Systems).

FRET experiments were performed on a confocal microscope (Bio-Rad 1024, krypton-argon laser 488 nm, 568 nm; Nikon Eclipse TE300, 40× oil immersion CFI Plan-Fluor numerical aperture 1.3 objective), using the GFP/DsRed couple as a donor/acceptor pair. A spectral parameter indicating the ability of donor/acceptor fluorescent molecules to exhibit efficient FRET is R_0, the Förster distance equal to the donor/acceptor separation at which FRET is 50% efficient. For the GFP/DsRed couple, this value is 5.7 nm (37), comparable with that reported for cyan fluorescent protein/yellow fluorescent protein, the leading pair for FRET experiments (38, 39). Fluorescent images of the donor were acquired by exciting GFP with the 488-nm line of the krypton-argon laser and detected using a 522 ± 35-nm filter. Images of the acceptor were acquired by exciting DsRed with the 568-nm line of the krypton-argon laser and detected with a 585-nm long pass filter. FRET was determined by the acceptor photobleaching method (40, 41). Briefly, after acquisition of an acceptor image (A1), a first Z-series of the donor (GFP) was acquired by scanning repeatedly with the 488-nm light of the confocal system (prebleach; D1). Then a region of interest of the cell was

photobleached at 568 nm with 100% laser power until all acceptor (DsRed) was photodestroyed (A2), and a second Z-series of the donor was acquired (postbleach; D2). After correction for image acquisition using the Amira software (TGS), maximum intensity projections from the Z-series of GFP images were generated. The FRET-dependent increase in fluorescence of the donor in the photobleached region was visualized by subtracting the prebleach GFP image from the postbleach GFP image (D2 − D1). For each experiment, FRET efficiencies in FA sites (E_{FA}) were calculated from the pre- and postbleach donor images according to the following equation: $E_{FA} = 1 - (I_{FA,\ prebleach}/I_{FA,\ postbleach})$, where I is the average intensity measured for the corresponding FA (41). For each cell analyzed, E_{FA} values were calculated for 4–8 FA sites in the photobleached region as well as in the control (nonbleached) region, and the results were expressed as means ± S.E.

Pull-down Assays—Platelets were isolated from freshly drawn whole blood as described previously (42) and lysed by sonication on ice in lysis buffer (50 mM NaCl, 150 mM sucrose, 10 mM Pipes, 1% Triton X-100, 0.5% deoxycholate, 1 mM EDTA, 1 mM Na_3VO_4, 50 mM NaF, 5 μg/ml aprotinin, 2.5 μg/ml leupeptin, and 1 mM phenylmethylsulfonyl fluoride, pH 6.8). Lysates were clarified by centrifugation at 4 °C for 30 min at 13,000 rpm, and protein concentration was determined using the Bio-Rad protein assay according to the manufacturer's instructions.

For direct protein-protein interaction assays, 200 μl of crude bacterial lysates containing the GST fusion proteins talin A, B, F, G, H, J, or K or GST alone were each mixed with 20 μl of glutathione-Sepharose beads for 1 h at 4 °C and subsequently washed four times with PBS plus 0.05% Tween 20. Sepharose beads coated with the different talin fragments were then incubated with 1 mg of platelet lysate for 2.5 h at 4 °C. Unbound proteins were washed off three times with PBS. Protein complexes were extracted in 25 μl of SDS-PAGE loading buffer (5 min, 100 °C) and separated on a 4–12% NuPAGE Bis-Tris gradient gel (Invitrogen). Western blot analysis of the transferred proteins was performed with a monoclonal anti-β_3 cytoplasmic tail antibody (C3a).

Surface Plasmon Resonance (SPR)—Measurements were performed on a Biacore3000 instrument (Biacore, Uppsala, Sweden). Goat anti-GST antibodies (Amersham Biosciences) were immobilized on a CM5 sensor chip according to the manufacturer's instructions (Biacore). Briefly, after activation of the carboxylate groups on the chip by a mixture of *N*-ethyl-*N*′-dimethylaminopropyl carbodiimide and *N*-hydroxysuccinimide (Biacore), a solution of 35 μg/ml goat anti-GST antibody in 10 mM acetate buffer (pH 4.9) was fluxed over the four channels of the chip for 7 min at a flow rate of 5 μl/min. The residual activated carboxylate groups were neutralized with 1 M ethanolamine (pH 8.5); for regeneration, 10 mM HCl was fluxed over the channels for 1 min.

For kinetic analysis, two channels were pretreated for 2 min at 5 μl/min with a 400 nM solution of recombinant GST (control channel) or GST-β_3 integrin constructs in a solution containing 150 mM NaCl, 10 mM Hepes, and 0.05% NP20 (HBS-N; Biacore). Subsequently, the purified recombinant talin fragment A or G, at a concentration ranging from 0.25 to 2 μM in HBS-N, was allowed to react with the two channels at a flow rate of 20 μl/min for 5 min, followed by a dissociation phase of 7.5 min. After each run, the channels were completely regenerated with 10 mM HCl. The obtained sensorgrams were analyzed with Biaeval 3.1 software (Biacore). Sensorgrams of the control channel were subtracted from the sensorgrams on the experimental channel and analyzed using nonlinear regression statistics to fit a simple Langmuir 1:1 binding model, taking into account the drifting base line, which is caused by the differential dissociation rate of GST alone and GST-β_3 from the anti-GST antibodies.

PAC-1 Binding Experiments and Flow Cytometry—Binding of the mouse antibody PAC-1, which is specific for the activated form of $\alpha_{IIb}\beta_3$ integrin, was assessed as previously described (36, 43). Briefly, ~5×10^5 cells in 50 μl of IMDM were preincubated for 20 min at room temperature in the presence or absence of the $\alpha_{IIb}\beta_3$-activating mouse antibody D3GP3 (3 μg). For control experiments, nonspecific binding of PAC-1 was assessed by incubating the cells in the presence of 1 mM RGDS peptide. PAC-1 antibody (3.5 μg in 50 μl of IMDM) was then directly added to the suspension, and cells were further incubated for 45 min at room temperature. Cells were washed in cold IMDM and incubated for 30 min on ice with a R-phycoerythrin-conjugated anti-mouse IgM antibody (Jackson ImmunoResearch Laboratories, Inc.), diluted in IMDM. Finally, cells were washed and resuspended in an appropriate buffer (137 mM NaCl, 5 mM KCl, 50 mM Hepes, 1 mg/ml glucose, pH 7.4). Flow cytometry was performed using a Coulter EPICS XL flow cytometer (Coulter, Hialeah, FL). After electronic compensation of the FL1 and FL2 fluorescence channels, PAC-1 binding (FL2) was analyzed on cells, which expressed the relevant GFP fusion proteins (FL1).

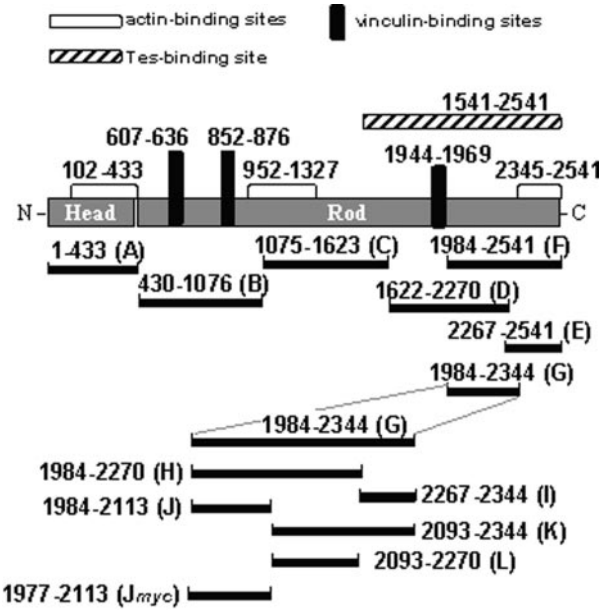

FIG. 1. **Schematic diagram of talin and the talin constructs used in this study.** The structure of talin and the location of major functional domains are indicated. The cytoskeletal protein talin (*gray bar*) is composed of an N-terminal head and a C-terminal rod domain. The positions of the three actin-binding sites (*open horizontal bars*), the three vinculin-binding sites (*filled vertical bars*), and the C-terminal rod domain sequence that harbors a TES-binding site (*hatched horizontal bar*) are indicated. The *horizontal filled bars* represent the different recombinant human talin1 fragments generated as fusion proteins with GST (*A*, *B*, *F*, *G*, *H*, *J*, and *K*), DsRed (*A*, *B*, *C*, *D*, *E*, *F*, *G*, *H*, *I*, *J*, *K*, and *L*) or with a *myc*-His tag (J_{myc}). The *numbers* represent the first and last amino acid of each fragment or binding site.

RESULTS

Subcellular Localization of Recombinant Talin Fragments Covering the Entire Amino Acid Sequence of Human talin1—We have previously shown that fusion of GFP to the cytoplasmic tail of the β_3 integrin subunit allowed surface expression of a fully functional $\alpha_{IIb}\beta_3$-GFP receptor (36). In order to characterize the β_3-binding site contained within the talin rod domain, we have used a fluorescence cell biology approach to identify DsRed-talin fragments that colocalize with β_3-GFP when expressed in CHO $\alpha_{IIb}\beta_3$-GFP cells. For this purpose, partially overlapping cDNA fragments encoding the entire amino acid sequence of human *talin1* were generated as outlined in Fig. 1 by reverse transcriptase-PCR using human erythroleukemic HEL cell mRNA as a template. Each amplified cDNA fragment was cloned into the pDsRed-N1 vector and verified by automated cDNA sequencing. The constructs were transiently transfected into CHO $\alpha_{IIb}\beta_3$-GFP cells, and the subcellular localization of each fragment in the cells, plated on fibrinogen, was analyzed by two-color fluorescence microscopy. Analysis was confined to cells expressing low levels of the tagged protein, because in cells overexpressing DsRed-tagged fusion proteins, the increased cytoplasmic staining obscured specific staining. As shown in Fig. 2, fragment A, which corresponds to the talin head domain and which contains a known integrin-binding site, and fragment B, which carries two vinculin-binding sites (44), both colocalized with β_3-GFP-stained adhesion structures at the cell periphery. The relatively small size of these structures as compared with larger mature FAs suggests that they represent focal complexes or early FAs. Fragment D exhibited a granular localization, distinct from FA labeling. This granular localization was also observed when talin fragment D was transfected into the human cancer cell line HT-144 (data not shown), suggesting the presence of a potential vesicle-targeting domain in this fragment. Fragment

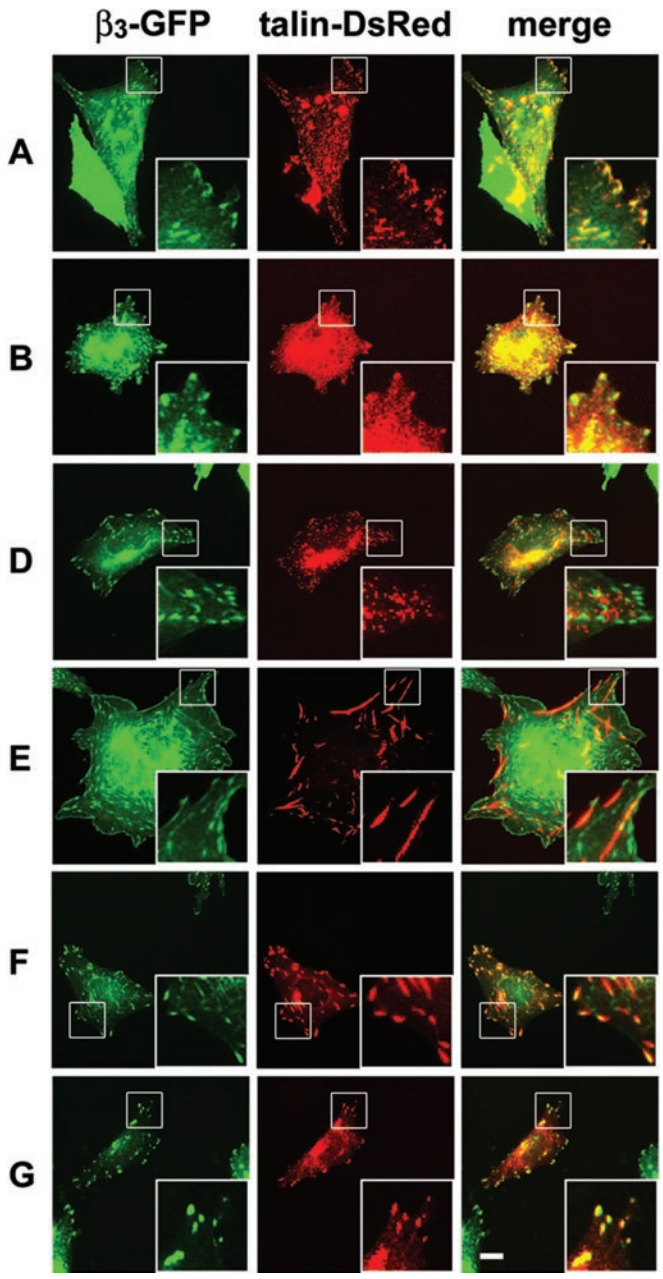

FIG. 2. **Subcellular localization of recombinant DsRed-talin fragments after transient expression in CHO $\alpha_{IIb}\beta_3$-GFP cells.** CHO cells expressing $\alpha_{IIb}\beta_3$-GFP were transiently transfected with cDNA encoding talin fragments A, B, D, E, F, and G, fused to DsRed. The transfected cells were detached, plated on fibrinogen-coated coverslips, and fixed with paraformaldehyde prior to observation under a conventional fluorescence microscope. For each talin fragment, β_3-GFP (*green*) and DsRed-talin (*red*) images were acquired and merged to visualize protein colocalization. The *insets* show a magnification of the area *boxed*. *Bar*, 10 μm.

F, which has previously been shown to interact with β_3 *in vitro* (29), colocalized with β_3 in FAs. Additionally, in cells expressing high levels of fragment F, we observed staining of actin filaments, emerging from β_3-GFP-containing FAs, most likely due to the actin-binding site within fragment F. In contrast, fragment E, which corresponds to the C-terminal part of the rod domain, co-localized with cortical actin filaments. We were unsuccessful in expressing fragment C, which corresponds to the central part of the rod domain and which carries the major part of an actin-binding site. Since fragments E and F both contain the conserved actin-binding sequence (I/L)WEQ of the C-terminal part of the rod domain (32), the subcellular localization of a shorter fragment G (amino acids 1984–2344), deleted of sequence corresponding to fragment E, was analyzed. Interestingly, fragment G clearly labeled mature FAs but not actin filaments, suggesting that this fragment could harbor a functional integrin-binding site.

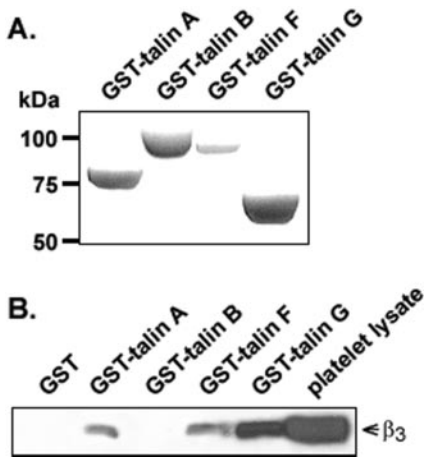

FIG. 3. ***In vitro* binding of the C-terminal part of the talin rod domain to the β_3 integrin subunit.** *A*, talin fragments A, B, F, and G were expressed as GST fusion proteins and purified by affinity chromatography on glutathione-Sepharose from crude bacterial lysates. Eluted GST fusion proteins were resolved on a gradient SDS-polyacrylamide gel and stained with Coomassie Blue. The apparent molecular masses corresponded to the calculated masses of 76 kDa (fragment A), 93 kDa (fragment B), 86 kDa (fragment F), and 66 kDa (fragment G). The positions of the molecular weight marker proteins are indicated. *B*, for β_3 pull-down assays, recombinant GST, used as a control, and GST-talin fragments A, B, F, and G were immobilized on glutathione-Sepharose and subsequently incubated with platelet lysate as described under "Experimental Procedures." Protein complexes or total platelet lysate (*last lane*) were resolved by gradient SDS-PAGE and transferred to a nitrocellulose membrane, and β_3 was revealed with the C3a monoclonal antibody directed against the cytoplasmic tail of β_3.

In Vitro Binding of the C-terminal Part of the Talin Rod Domain to the β_3 Integrin Subunit—To elucidate whether fragment G was able to interact with β_3 *in vitro*, we performed pull-down experiments of $\alpha_{IIb}\beta_3$ from platelet lysate using recombinant talin fragments. Talin fragments A, B, F, and G were expressed as GST fusion proteins and purified on glutathione-Sepharose, and their calculated masses of 76, 93, 86, and 66 kDa, respectively, were confirmed by SDS-PAGE analysis (Fig. 3*A*). For protein-protein interaction experiments, the GST-talin fragments or GST alone were immobilized on glutathione-Sepharose and used to precipitate $\alpha_{IIb}\beta_3$ from platelet lysate. As shown in Fig. 3*B*, only the talin rod domain fragments F and G, but not B, were able to trap $\alpha_{IIb}\beta_3$, clearly indicating that fragment G contains the C-terminal β_3-binding site of the rod domain. Experiments with the talin head domain fragment A or GST alone served as positive and negative controls, respectively. These data also provide evidence that the observed FA localization of fragment B, which corresponds to the N-terminal part of the rod domain and contains two vinculin-binding sites, was probably due to interaction with vinculin rather than with integrins.

SPR Analysis of the Direct Protein-Protein Interaction between the Rod Domain Fragment G and the β_3 Cytoplasmic Tail—Since a talin fragment encompassing residues 1541–2541 has recently been shown to contain a binding site for the FA protein TES (31) and to exclude that pull-down of $\alpha_{IIb}\beta_3$ by fragment G was mediated indirectly through this talin-binding protein TES, we performed SPR analysis using recombinant GST-β_3 cytoplasmic tail fusion proteins as ligands and recombinant talin A and talin G fragments, deleted of the GST moiety, as analytes. Fig. 4*A* shows the purified recombinant

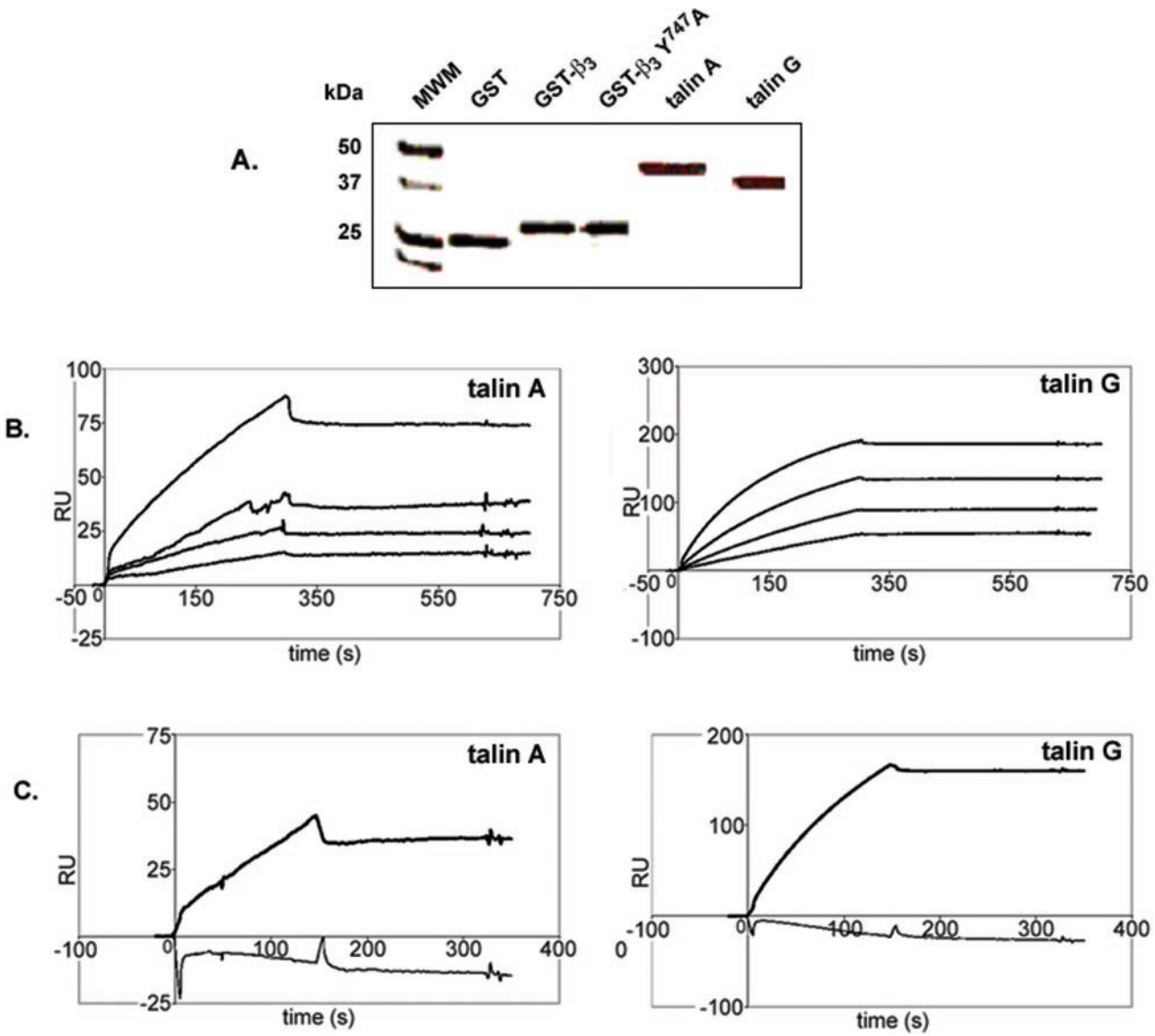

FIG. 4. **SPR analysis of the direct protein-protein interaction between the rod domain fragment G and the β_3 cytoplasmic tail.** *A*, recombinant GST fusion proteins of the wild type and mutant (Y747A) β_3 cytoplasmic tail and GST fusion proteins of talin fragments A and G were expressed in *E. coli* and purified from bacterial lysates by affinity chromatography on glutathione-Sepharose. GST-talin fragments A and G were cleaved from the GST tag by thrombin digestion on the glutathione-Sepharose. Eluted proteins GST, GST-β_3, and GST-β_3Y747A and the talin fragments A and G were dialyzed against PBS, resolved by gradient SDS-PAGE, and stained with Coomassie Blue. The position of the molecular weight marker proteins (*MWM*) is indicated on the *left*. *B*, recombinant wild type GST-β_3 tail protein was captured on a sensor chip, where anti-GST antibodies had been previously immobilized. Talin fragments A (*left panel*) or G (*right panel*) (0.25, 0.5, 1, and 2 μM from the *lower trace*) were then injected at a flow rate of 20 μl/min, as described under "Experimental Procedures." Injecting buffer without dissolved proteins started the dissociation phase. *C*, sensorgrams of association and dissociation phase for binding of the talin fragments A (*left panel*) and G (*right panel*) to the wild type GST-β_3 (*thick line*) and mutant (Y747A) GST-β_3 (*thin line*) tail proteins, immobilized on an anti-GST-coated sensor chip.

proteins following SDS-PAGE analysis and demonstrates the absence of cleaved GST in the samples corresponding to the talin fragments A and G. β_3 integrin constructs were captured on immobilized anti-GST antibodies, resulting in a homogeneous orientation of the ligand. The sensorgrams for the interaction of increasing concentrations of talin fragments A and G with wild type GST-β_3 are shown in Fig. 4*B*. Calculation of the association rate constants for the talin A- and talin G-β_3 interactions gave values of $1.5 \pm 0.8 \times 10^3$ M^{-1} s^{-1} and $4.0 \pm 0.3 \times 10^3$ M^{-1} s^{-1}, respectively. These low association rate constants could point to the necessity of conformational changes for the formation of a stable integrin-talin complex or to the overevaluation of the concentration of active talin fragments, since the protein concentration does not always correspond to the concentration of interacting molecules. Nevertheless, the association rate constants for both talin A and talin G were very similar. On the other hand, the dissociation rate constant for talin A ($9.7 \pm 1.6 \times 10^{-6}$ s^{-1}) was much lower than that for talin G ($6.3 \pm 6.2 \times 10^{-4}$ s^{-1}), yielding dissociation equilibrium constants of 7.7 and 157 nM, respectively. These data demonstrate a direct interaction of talin fragment G with the cytoplasmic tail of β_3, although with a lower binding affinity than that measured for talin fragment A. Interestingly, neither fragment A nor fragment G interacted with the GST-β_3 cytoplasmic tail mutant Y747A at the highest concentration used (2 μM), suggesting that the β_3 integrin-binding sites for the talin head and the talin rod domain are in close proximity and that both interactions rely on the presence of residue Tyr^{747}. The observation of a quasi-irreversible dissociation results from two dissociations: the real dissociation rate of the talin fragments from the integrin cytoplasmic tails and the differential dissociation of the control GST and GST-β_3 from the anti-GST antibodies

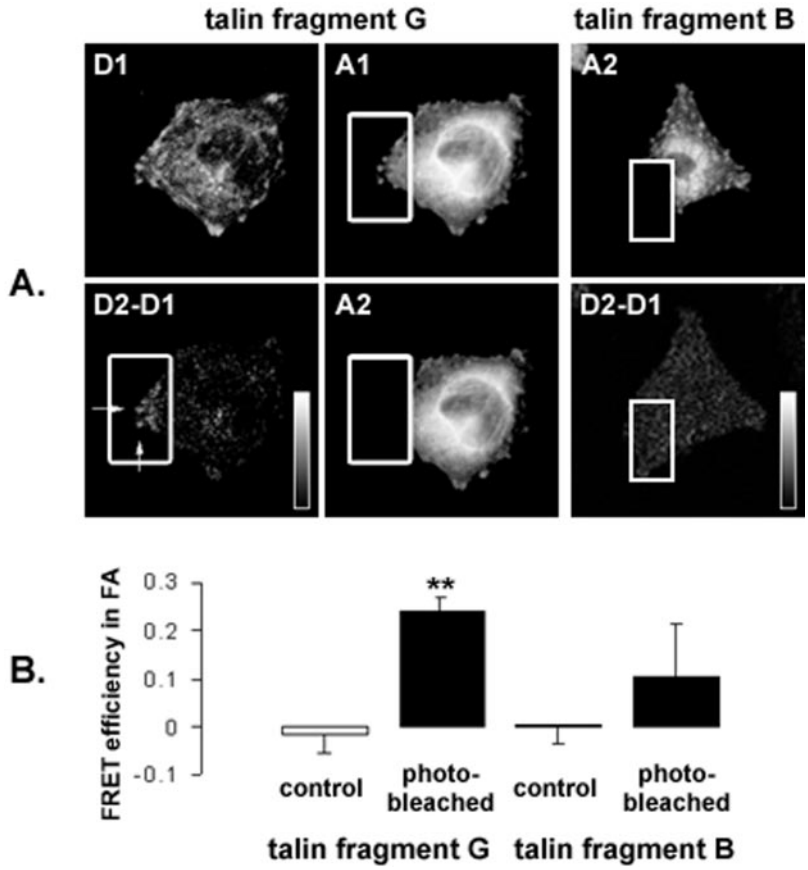

FIG. 5. **FRET detection of the molecular association of β_3-GFP with DsRed-talin fragment G in focal adhesions of CHO $\alpha_{IIb}\beta_3$-GFP cells.** *A*, *in situ* FRET analysis was performed on a confocal microscope using CHO $\alpha_{IIb}\beta_3$-GFP cells that transiently expressed DsRed-talin fragments B and G. Transfected cells were plated onto fibrinogen-coated coverslips and fixed prior to image acquisition. A donor image (β_3-GFP; *D1*) and acceptor image (DsRed-talin fragment; *A1*) were acquired before photobleaching of the acceptor in a defined area of the cell by continuous scanning with the 568-nm laser line (full power). After photodestruction of the acceptor (*A2*; *white rectangle*), a second donor image was acquired, and a *difference image* (*D2-D1*) was generated. The decrease of FRET between β_3-GFP and DsRed-talin fragment G after acceptor photobleaching is seen on the *difference image* (*D2-D1*) as an increase of donor fluorescence intensity (*white arrows*) in the photobleached region as compared with the control region. This increase is not observed in the difference image (*D2-D1*) for DsRed-talin fragment B. *B*, for both fragment G- and fragment B-expressing cells, FRET efficiency was calculated in FAs of the photobleached and of the control region and was expressed as mean ± S.E. **, $p < 0.003$, significantly different from control.

immobilized on the chip. To distinguish the real talin-integrin dissociation rate, a single Langmuir model was chosen, including a drifting base line, which takes the GST- anti-GST dissociation into account.

FRET Detection of the Molecular Association of β_3-GFP with DsRed-talin Fragment G in Focal Adhesions of CHO $\alpha_{IIb}\beta_3$-GFP Cells—To confirm that colocalization of the talin rod domain fragment G with the β_3 cytoplasmic tail within the cell is physiologically relevant and corresponds to a true protein-protein interaction, *in situ* FRET experiments were performed using GFP fused to the β_3 integrin cytoplasmic tail as the donor and DsRed fused to different talin fragments (fragments B and G) as the acceptor. CHO $\alpha_{IIb}\beta_3$-GFP cells were transiently transfected with DsRed-fused talin fragments B and G and allowed to adhere to fibrinogen, and FRET analysis was performed on a confocal microscope by comparing the images of donor emission (GFP), excited at 488 nm before (D1) and after (D2) acceptor (DsRed) photobleaching. In 15% of the cells transfected with talin fragment G, a decrease in FRET could be detected as a clear increase in donor emission intensity after photobleaching of the acceptor (Fig. 5*A*, *D2-D1*). In cells exhibiting this change in FRET, higher amounts of acceptor were expressed so that DsRed-talin fragment G staining was observed not only in FAs but also in the cytoplasm, indicating that the quantity of acceptor is a limiting factor in this approach. However, an increase in donor fluorescence was only detected in FAs (Fig. 5*A*, *arrows*), demonstrating that in CHO $\alpha_{IIb}\beta_3$-GFP cells, talin fragment G is in very close contact with the cytoplasmic tail of β_3. In contrast, photobleaching of DsRed-talin fragment B (Fig. 6*A*) or DsRed-talin fragment A (data not shown) resulted in no significant increase of donor fluorescence intensity in all cells analyzed. However, it is generally not possible to interpret negative FRET results unless the spatial orientation of the donor and acceptor molecules is controlled (45). Observations made on the difference (*D2-D1*) images were quantified by calculating FRET efficiencies in FA sites as described under "Experimental Procedures." A significant difference of FRET efficiency could be observed between the photobleached and the control (nonbleached) region for cells expressing DsRed-talin fragment G ($p = 0.0024$) but not for cells expressing DsRed-talin fragment B ($p = 0.4261$) (Fig. 5*B*). These results clearly show that the DsRed-talin fragment G is in very close contact with β_3-GFP and suggest that the two proteins do interact directly within FAs.

Delimitation of the β_3 Integrin-binding Site to a 130-Residue Sequence within the Talin Rod Domain—To further map out the integrin-binding site within the amino acid sequence of talin fragment G, five overlapping cDNA fragments (fragments H, I, J, K, and L) were generated (Fig. 1) and expressed as DsRed fusion proteins in CHO $\alpha_{IIb}\beta_3$-GFP cells. As shown in Fig. 6*A*, two overlapping talin fragments, H (287 amino acids) and J (130 amino acids), localized in FAs, whereas the other three fragments (fragments I, K, and L) displayed diffuse cytoplasmic staining, suggesting that the β_3 integrin-binding sequence is comprised within residues 1984–2113 of fragment J.

Since DsRed has previously been shown to aggregate and form oligomers (46) and in order to exclude potential nonspecific clustering of DsRed fusion proteins in FA plaques, we performed a control experiment by generating a cDNA construct (J_{myc}; Fig. 1), similar to fragment J, but devoid of DsRed and instead fused to a *myc*-His tag. Indirect immunofluorescence labeling of the transfected CHO $\alpha_{IIb}\beta_3$-GFP cells with an anti-*myc* antibody and a rhodamine-conjugated secondary antibody displayed the same FA staining pattern for talin fragment J_{myc} (Fig. 6*B*) as for DsRed-talin fragment J (Fig. 6*A*).

Finally, we performed pull-down experiments of $\alpha_{IIb}\beta_3$ using purified GST-fused talin fragments G (66 kDa), H (60 kDa), J (37 kDa), and K (50 kDa) (Fig. 6*C*). As shown in Fig. 6*D*, talin

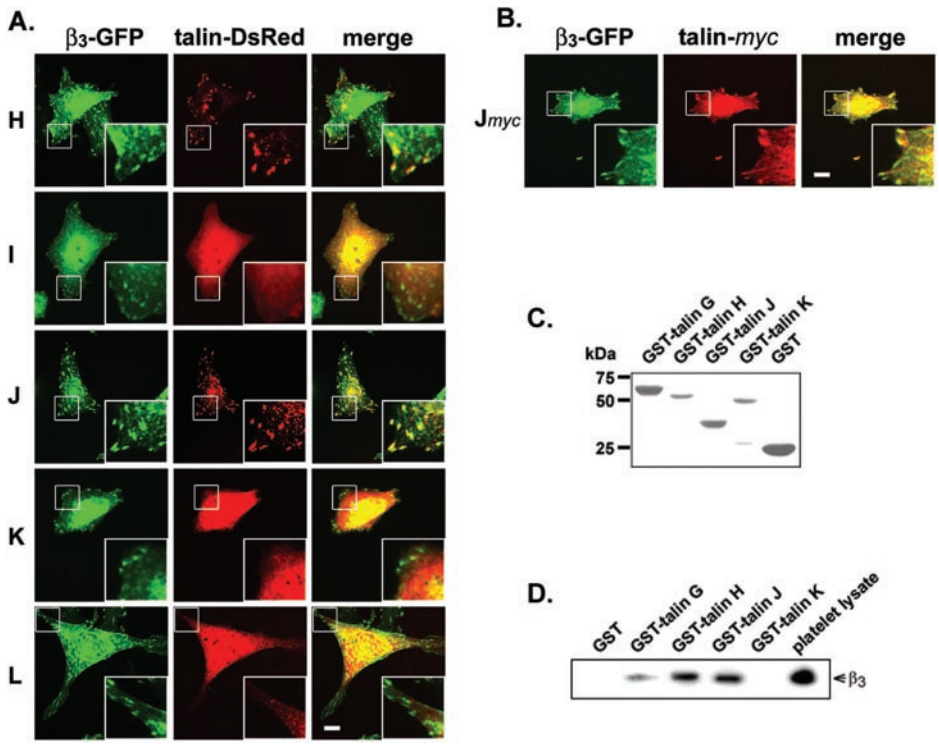

FIG. 6. **Delimitation of the β_3 integrin-binding site within fragment G of talin.** *A*, five overlapping DsRed-talin fragments (fragments H, I, J, K, and L), covering the sequence of talin G, were transiently expressed in CHO $\alpha_{IIb}\beta_3$-GFP cells. The transfected cells were detached, plated on fibrinogen-coated coverslips, and fixed prior to observation under a conventional fluorescence microscope. For each talin fragment, GFP-β_3 and DsRed-talin images were acquired and merged to visualize protein colocalization. The *insets* show a magnification of the area *boxed*. *Bar*, 10 μm. *B*, the subcellular localization of the *myc*-His-tagged talin fragment J (J_{myc}), was visualized with an anti-*myc* monoclonal mouse antibody and rhodamine-conjugated goat anti-mouse IgG antibody. *Bar*, 10 μm. *C*, talin fragments G, H, J, and K were expressed as GST fusion proteins and analyzed as described in the legend to Fig. 3*A*. The apparent molecular masses corresponded to the calculated weights of 66 kDa (*G*), 60 kDa (*H*), 37 kDa (*J*), and 50 kDa (*K*). *D*, pull-down of β_3 from platelet lysate using GST-talin fragments G, H, J, and K was performed as outlined in the legend to Fig. 3*B*.

fragments G, H, and J, but not fragment K, were able to precipitate $\alpha_{IIb}\beta_3$ from platelet lysate, demonstrating that the amino acid sequence 1984–2113 of the talin rod domain contains a functional β_3 integrin-binding site.

Interaction of the Talin Rod Domain Fragment G with $\alpha_{IIb}\beta_3$ Does Not Induce Integrin Activation—Recent data have shown that recombinant talin head domain fragments, which contain the integrin-binding site, activate $\alpha_{IIb}\beta_3$ when overexpressed in CHO $\alpha_{IIb}\beta_3$ cells (7, 24), whereas down-regulation of talin prevents integrin activation (8). To elucidate whether the integrin-binding site in the talin rod domain also participates in integrin activation, we generated cDNAs encoding GFP-fused talin fragments A and G and transiently transfected them into CHO cells stably expressing $\alpha_{IIb}\beta_3$ (35). The activation state of $\alpha_{IIb}\beta_3$ was assessed in flow cytometry by measuring the binding of the activation-specific anti-$\alpha_{IIb}\beta_3$ antibody PAC-1 (43). Fig. 7 shows that cells expressing the GFP-fused integrin-binding fragment G of the talin rod domain (GFP-talin G) did not display increased PAC-1 binding in contrast to cells expressing the GFP-fused talin head domain (GFP-talin A) as demonstrated by the vertical upward shift of the transfected cell population in the density plot. Maximal PAC-1 binding was assessed using the $\alpha_{IIb}\beta_3$-activating antibody D3GP3, and specificity of PAC-1 binding was confirmed using an RGDS peptide, which completely abrogated PAC-1 binding. Increased PAC-1 binding was not observed in cells expressing GFP alone (data not shown). These data provide evidence that, unlike the talin head domain, binding of the talin rod domain fragment G to the cytoplasmic tail of β_3 does not participate in the activation of $\alpha_{IIb}\beta_3$.

DISCUSSION

Talin is a multifunctional cytosolic actin-binding protein that plays a major role in linking integrins to the actin cytoskeleton. It is therefore not surprising that talin contains, in addition to its three actin-binding sites (18), multiple redundant functional domains, notably three binding sites for acidic phospholipids (47), three vinculin-binding sites (30), a binding site for the recently identified focal adhesion protein TES (31), and two integrin-binding sites (3, 24, 29). In the present study, we have delimited the second integrin-binding site of talin to a sequence of 130 residues in the rod domain and have demonstrated the *in vivo* relevance of this interaction using a cell biology approach and fluorescence energy transfer.

Overlapping DsRed-tagged fragments covering the entire amino acid sequence of talin were expressed in CHO $\alpha_{IIb}\beta_3$-GFP cells to study subcellular localization patterns of the different recombinant proteins. This way, we have mapped out the second integrin-binding site of talin to residues 1984–2113 in the C-terminal part of the rod domain, located between the highly conserved (I/L)WEQ actin-binding domain (residues 2345–2541) and the third vinculin-binding site (residues 1944–1969). The distinct subcellular staining of the transiently expressed DsRed-talin fragments in CHO $\alpha_{IIb}\beta_3$-GFP cells of either FAs, actin filaments, or granular structures underlines the reliability of the approach and excludes artifactual or nonspecific clustering of the recombinant fusion proteins due to the presence of the DsRed tag (46). Also, the specificity of the subcellular localization of fragment J was further confirmed with the expression of a similar fragment (J_{myc}), fused to a *myc*-His tag and devoid of the DsRed moiety.

A result of interest was the subcellular localization of the fragments that contained, in addition to the β_3 integrin-binding site, a second functional domain such as the C-terminal actin-binding site (fragment F) or a potential new vesicle targeting domain (fragment D). Fragment F was localized in FAs when expressed at low levels and localized along actin filaments, emerging from FAs, when expressed at higher levels, suggesting a lower affinity of the actin-binding motif as compared with the integrin-binding site of the talin rod domain. Fragment D labeled granular structures, which may imply an involvement of talin in vesicle transport processes. Although the significance of this localization remains to be investigated, these data are reminiscent of findings showing that down-regulation of talin either by an antisense (12) or by a gene targeting approach (48) compromised integrin trafficking and

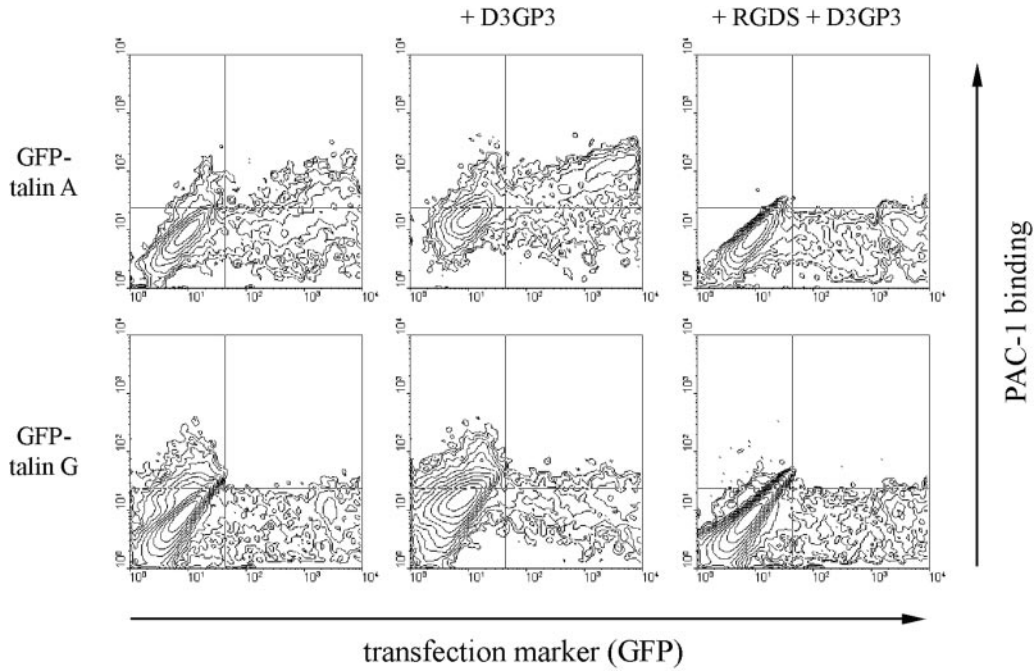

FIG. 7. **Interaction of the talin rod domain fragment G with $\alpha_{IIb}\beta_3$ does not induce integrin activation.** CHO $\alpha_{IIb}\beta_3$ cells were transiently transfected with cDNAs encoding GFP-fused talin fragment A or G. 24 h after transfection, binding of the activation-specific anti-$\alpha_{IIb}\beta_3$ mouse antibody PAC-1 (*y* axis) and GFP fluorescence (*x* axis) were assessed by flow cytometry. *Contour plots* of cells transiently expressing the indicated recombinant proteins in absence or presence of the $\alpha_{IIb}\beta_3$-activating antibody D3GP3 are shown. Nonspecific binding of PAC-1 was examined in the presence of 1 mM RGDS peptide. Data are representative of at least three independent experiments.

surface expression and led to a marked change in the actin cytoarchitecture.

The talin rod domain was initially identified as the integrin-binding domain (3), and subsequent *in vitro* binding studies localized this binding site to the 558 C-terminal amino acids of talin (residues 1984–2541) (29). Our data precisely delimit this integrin-binding site to a small fragment of 130 amino acids (residues 1984–2113 of talin fragment J). In the absence of any notable sequence similarity of fragment J with the FERM domain of the talin head, the binding mechanism, the binding site, and the affinity of the rod domain for the β_3 tail are likely to be different from that recently reported for the talin head domain (25). We used real time SPR to demonstrate the *in vitro* interaction of the recombinant talin fragments (A and G) with the β_3 cytoplasmic tail and determined the respective binding affinities corresponding to a K_d of 7.7 nM for the head domain fragment A and 157 nM for the rod domain fragment G. Even if we consider the possibility that not all recombinant talin molecules are interacting molecules, the very low association rate constants for both fragment A and fragment G with the β_3 integrin cytoplasmic tail suggest that the formation of a stable complex requires conformational changes in one or both of the interacting partners. The difference in β_3 integrin affinity for the talin head and rod domain, which has already been observed by Yan *et al.* (23), is thus essentially due to a difference in the dissociation rate constant, which is 65 times lower for fragment A as compared with fragment G. The 10-fold difference in the affinity of the talin head domain for β_3 reported here as compared with the data reported by Yan *et al.* (23) is most likely due to differences in the experimental setting, notably the species origin of the talin head domain (human *versus* mouse) and the β_3 cytoplasmic tail construct (GST-β_3 fusion protein *versus* a biotin-maleimide-labeled model protein containing a four-heptad repeat motif and a spacer of 4 glycines linked to the N-terminal part of the β_3 cytoplasmic tail). Since the β_3Y747A mutation abolished the interaction of the mutant β_3 subunit cytoplasmic tail with both fragment A and fragment G, we conclude that the talin head and rod domains recognize either one or two closely proximal sites in β_3, suggesting a mutually exclusive interaction of the two domains with the β_3 cytoplasmic tail rather than a cooperative binding (23).

Taking advantage of the GFP/DsRed pair of autofluorescent tags, we have shown fluorescence resonance energy transfer between β_3-GFP and DsRed-fused talin fragment G, which emphasizes the *in vivo* relevance of the talin rod domain interaction with β_3. FRET measurements were possible, since the FRET pair GFP/DsRed exhibits good wavelength separation of donor and acceptor emission spectra. Moreover, the spectral characteristics of GFP allow the use of the 568-nm line of the krypton/argon laser to excite DsRed with no excitation of GFP, a condition required when using the acceptor photobleaching method to assess FRET. However, measured FRET efficiency was low, and FRET could only be detected in ~15% of the cells expressing talin fragment G. This can be explained by the fact that in CHO $\alpha_{IIb}\beta$3-GFP cells, the transfected DsRed-talin fragments compete with endogenous talin for interacting with the different binding partners. Since the analyzed cells were attached and spread, it can be assumed that a major part of the β_3-GFP cytoplasmic tails was still bound to endogenous talin, thus decreasing the ratio between the acceptor (DsRed-talin fragment) and the donor (β_3-GFP cytoplasmic tail) in FAs so that FRET efficiency was diminished. Other factors that influence FRET efficiency are the slow chromophore maturation of DsRed of typically 48 h to reach 90% of maximum fluorescence (49) as well as the orientation and the total amount of fluorescent proteins within the cell (45). Therefore, it is difficult to interpret negative FRET results as in the case of talin fragments A and B.

Several studies have conclusively established the functional role of the talin head domain in inside-out signaling as such that it mediates spatial separation of the α and β cytoplasmic domains, which subsequently leads to integrin activation (7, 8, 24–26, 50). Using the activation-specific PAC-1 antibody, we demonstrated that, unlike the talin head domain, the rod do-

main fragment G by itself is unable to activate $\alpha_{IIb}\beta_3$. Although the talin rod domain has recently been shown to activate vinculin (51, 52), which suggests a regulatory role in FA assembly, its exact function in binding to integrins remains to be investigated further. However, a direct role in outside-in signaling appears likely, where interaction of the rod domain with numerous cytoskeletal proteins such as vinculin, actin, and the newly identified TES protein may account for the clustering of integrins by strengthening the link between integrins and the actin cytoskeleton in mature FAs. This hypothesis is supported by the observation that the transfected talin head domain was localized in relatively small structures on the cell periphery that resembled focal complexes or early FAs rather than mature FAs, whereas talin fragments containing the rod domain integrin-binding site (fragments F, G, H, J, and J_{myc}) labeled larger mature FAs. The Tyr^{747} of the β_3 cytoplasmic tail seems to be required for both talin head and rod domain binding, and this suggests a mutually exclusive interaction. It can be speculated that after activation of the receptor, the talin head domain is replaced from the β_3 cytoplasmic tail by the rod domain, which then exerts its function in events downstream of activation, such as clustering of integrins and maturation of FAs. Considering that binding of talin to integrins is the general and final step in signaling events that lead to integrin activation (8), it will be of importance to precisely determine the temporal and functional role of the talin rod domain in signaling cascades that regulate the behavior of activated integrins.

Acknowledgments—We thank Dr. D. R. Phillips and Dr. L. K. Jennings for providing the antibodies C3a and D3GP3, respectively. We acknowledge the expertise of Snezana Mancic (IFR85, Illkirch, France) for image analysis in FRET experiments.

REFERENCES

1. Shimaoka, M., and Springer, T. A. (2003) *Nat. Rev. Drug Discov.* **2,** 703–716
2. Liu, S., Calderwood, D. A., and Ginsberg, M. H. (2000) *J. Cell Sci.* **113,** 3563–3571
3. Horwitz, A., Duggan, K., Buck, C., Beckerle, M. C., and Burridge, K. (1986) *Nature* **320,** 531–533
4. Goldmann, W. H., Bremer, A., Haner, M., Aebi, U., and Isenberg, G. (1994) *J. Struct. Biol.* **112,** 3–10
5. Molony, L., McCaslin, D., Abernethy, J., Paschal, B., and Burridge, K. (1987) *J. Biol. Chem.* **262,** 7790–7795
6. Calderwood, D. A., and Ginsberg, M. H. (2003) *Nat. Cell Biol.* **5,** 694–697
7. Calderwood, D. A., Yan, B., de Pereda, J. M., Alvarez, B. G., Fujioka, Y., Liddington, R. C., and Ginsberg, M. H. (2002) *J. Biol. Chem.* **277,** 21749–21758
8. Tadokoro, S., Shattil, S. J., Eto, K., Tai, V., Liddington, R. C., de Pereda, J. M., Ginsberg, M. H., and Calderwood, D. A. (2003) *Science* **302,** 103–106
9. Burridge, K., and Connell, L. (1983) *J. Cell Biol.* **97,** 359–367
10. DePasquale, J. A., and Izzard, C. S. (1991) *J. Cell Biol.* **113,** 1351–1359
11. Nuckolls, G. H., Romer, L. H., and Burridge, K. (1992) *J. Cell Sci.* **102,** 753–762
12. Albiges-Rizo, C., Frachet, P., and Block, M. R. (1995) *J. Cell Sci.* **108,** 3317–3329
13. Martel, V., Racaud-Sultan, C., Dupe, S., Marie, C., Paulhe, F., Galmiche, A., Block, M. R., and Albiges-Rizo, C. (2001) *J. Biol. Chem.* **276,** 21217–21227
14. Monkley, S. J., Zhou, X. H., Kingston, S. J., Giblett, S. M., Hemmings, L., Priddle, H., Brown, J. E., Pritchard, C. A., Critchley, D. R., and Fassler, R. (2000) *Dev. Dyn.* **219,** 560–574
15. Monkley, S. J., Pritchard, C. A., and Critchley, D. R. (2001) *Biochem. Biophys. Res. Commun.* **286,** 880–885
16. Brown, N. H., Gregory, S. L., Rickoll, W. L., Fessler, L. I., Prout, M., White, R. A., and Fristrom, J. W. (2002) *Dev. Cell* **3,** 569–579
17. Rees, D. J., Ades, S. E., Singer, S. J., and Hynes, R. O. (1990) *Nature* **347,** 685–689
18. Hemmings, L., Rees, D. J., Ohanian, V., Bolton, S. J., Gilmore, A. P., Patel, B., Priddle, H., Trevithick, J. E., Hynes, R. O., and Critchley, D. R. (1996) *J. Cell Sci.* **109,** 2715–2726
19. Niggli, V., Kaufmann, S., Goldmann, W. H., Weber, T., and Isenberg, G. (1994) *Eur. J. Biochem.* **224,** 951–957
20. Seelig, A., Blatter, X. L., Frentzel, A., and Isenberg, G. (2000) *J. Biol. Chem.* **275,** 17954–17961
21. Critchley, D. R. (2000) *Curr. Opin. Cell Biol.* **12,** 133–139
22. Barsukov, I. L., Prescot, A., Bate, N., Patel, B., Floyd, D. N., Bhanji, N., Bagshaw, C. R., Letinic, K., Di Paolo, G., De Camilli, P., Roberts, G. C., and Critchley, D. R. (2003) *J. Biol. Chem.* **278,** 31202–31209
23. Yan, B., Calderwood, D. A., Yaspan, B., and Ginsberg, M. H. (2001) *J. Biol. Chem.* **276,** 28164–28170
24. Calderwood, D. A., Zent, R., Grant, R., Rees, D. J., Hynes, R. O., and Ginsberg, M. H. (1999) *J. Biol. Chem.* **274,** 28071–28074
25. Garcia-Alvarez, B., de Pereda, J. M., Calderwood, D. A., Ulmer, T. S., Critchley, D., Campbell, I. D., Ginsberg, M. H., and Liddington, R. C. (2003) *Mol. Cell* **11,** 49–58
26. Ulmer, T. S., Calderwood, D. A., Ginsberg, M. H., and Campbell, I. D. (2003) *Biochemistry* **42,** 8307–8312
27. McLachlan, A. D., Stewart, M., Hynes, R. O., and Rees, D. J. (1994) *J. Mol. Biol.* **235,** 1278–1290
28. Winkler, J., Lunsdorf, H., and Jockusch, B. M. (1997) *Eur. J. Biochem.* **243,** 430–436
29. Xing, B., Jedsadayanmata, A., and Lam, S. C. (2001) *J. Biol. Chem.* **276,** 44373–44378
30. Gilmore, A. P., Wood, C., Ohanian, V., Jackson, P., Patel, B., Rees, D. J., Hynes, R. O., and Critchley, D. R. (1993) *J. Cell Biol.* **122,** 337–347
31. Coutts, A. S., MacKenzie, E., Griffith, E., and Black, D. M. (2002) *J. Cell Sci.* **116,** 897–906
32. McCann, R. O., and Craig, S. W. (1997) *Proc. Natl. Acad. Sci. U. S. A.* **94,** 5679–5684
33. McCann, R. O., and Craig, S. W. (1999) *Biochem. Biophys. Res. Commun.* **266,** 135–140
34. Woodside, D. G., Obergfell, A., Talapatra, A., Calderwood, D. A., Shattil, S. J., and Ginsberg, M. H. (2002) *J. Biol. Chem.* **277,** 39401–39408
35. Schaffner-Reckinger, E., Gouon, V., Melchior, C., Plançon, S., and Kieffer, N. (1998) *J. Biol. Chem.* **273,** 12623–12632
36. Plançon, S., Morel-Kopp, M. C., Schaffner-Reckinger, E., Chen, P., and Kieffer, N. (2001) *Biochem. J.* **357,** 529–536
37. Erickson, M. G. (2003) *Biophys. J.* **85,** 599–611
38. Miyawaki, A., Llopis, J., Heim, R., J. M., M., Adams, J. A., Ikura, M., and Tsien, R. Y. (1997) *Nature* **388,** 882–887
39. Patterson, G. H., Piston, D. W., and Barisas, B. G. (2000) *Anal. Biochem.* **284,** 438–440
40. Bastiaens, P. I., and Jovin, T. M. (1996) *Proc. Natl. Acad. Sci. U. S. A.* **93,** 8407–8412
41. Wouters, F. S., Bastiaens, P. I., Wirtz, K. W., and Jovin, T. M. (1998) *EMBO J.* **17,** 7179–7189
42. Pfaff, M., Liu, S., Erle, D. J., and Ginsberg, M. H. (1998) *J. Biol. Chem.* **273,** 6104–6109
43. O'Toole, T. E., Katagiri, Y., Faull, R. J., Peter, K., Tamura, R., Quaranta, V., Loftus, J. C., Shattil, S. J., and Ginsberg, M. H. (1994) *J. Cell Biol.* **124,** 1047–1059
44. Bass, M. D., Smith, B. J., Prigent, S. A., and Critchley, D. R. (1999) *Biochem. J.* **341,** 257–263
45. Berney, C., and Danuser, G. (2003) *Biophys. J.* **84,** 3992–4010
46. Mizuno, H., Sawano, A., Eli, P., Hama, H., and Miyawaki, A. (2001) *Biochemistry* **40,** 2502–2510
47. Isenberg, G., and Goldmann, W. H. (1998) *FEBS Lett.* **426,** 165–170
48. Priddle, H., Hemmings, L., Monkley, S., Woods, A., Patel, B., Sutton, D., Dunn, G. A., Zicha, D., and Critchley, D. R. (1998) *J. Cell Biol.* **142,** 1121–1133
49. Baird, G. S., Zacharias, D. A., and Tsien, R. Y. (2000) *Proc. Natl. Acad. Sci. U. S. A.* **97,** 11984–11989
50. Kim, M., Carman, C. V., and Springer, T. A. (2003) *Science* **301,** 1720–1725
51. Bass, M. D., Patel, B., Barsukov, I. G., Fillingham, I. J., Mason, R., Smith, B. J., Bagshaw, C. R., and Critchley, D. R. (2002) *Biochem. J.* **362,** 761–768
52. Izard, T., Evans, G., Borgon, R. A., Rush, C. L., Bricon, G., and Bois, P. R. (2004) *Nature* **427,** 171–175

A Fluorescence Cell Biology Approach to Map the Second Integrin-binding Site of Talin to a 130-Amino Acid Sequence within the Rod Domain

Laurent Tremuth, Stephanie Kreis, Chantal Melchior, Johan Hoebeke, Philippe Rondé, Sébastien Plançon, Kenneth Takeda and Nelly Kieffer

J. Biol. Chem. 2004, 279:22258-22266.
doi: 10.1074/jbc.M400947200 originally published online March 18, 2004
